Abscopal Gene Expression in Response to Synchrotron Radiation Indicates a Role for Immunological and DNA Damage Response Genes

Authors: Forrester, Helen B., Lobachevsky, Pavel N., Stevenson, Andrew W., Hall, Christopher J., Martin, Olga A., et al.

Source: Radiation Research, 194(6) : 678-687

Published By: Radiation Research Society

URL: https://doi.org/10.1667/RADE-19-00014.1

RADIATION RESEARCH **194**, 678–687 (2020)
0033-7587/20 $15.00

DOI: 10.1667/RADE-19-00014.1

Abscopal Gene Expression in Response to Synchrotron Radiation Indicates a Role for Immunological and DNA Damage Response Genes

Helen B. Forrester,[a,b,c,1] Pavel N. Lobachevsky,[d,f,g] Andrew W. Stevenson,[h,i] Christopher J. Hall,[h] Olga A. Martin[e,f,2] and Carl N. Sprung[a,b,2]

[a] *Centre for Innate Immunity and Infectious Diseases, Hudson Institute of Medical Research, Clayton, Australia;* [b] *Monash University, Clayton, Australia;* [c] *School of Science, RMIT University, Melbourne, Australia;* [d] *Research Division and* [e] *Division of Radiation Oncology, Peter MacCallum Cancer Centre, Melbourne, Australia;* [f] *Sir Peter MacCallum Department of Oncology, The University of Melbourne, Melbourne, Australia;* [g] *Advanced Analytical Technologies, Melbourne, Australia;* [h] *Australian Synchrotron, ANSTO, Clayton, Australia; and* [i] *CSIRO Manufacturing, Clayton, Australia*

Forrester, H. B., Lobachevsky, P. N., Stevenson, A. W., Hall, C. J., Martin, O. A. and Sprung, C. N. Abscopal Gene Expression in Response to Synchrotron Radiation Indicates a Role for Immunological and DNA Damage Response Genes. ***Radiat. Res.*** **194, 678–687 (2020).**

Abscopal effects are an important aspect of targeted radiation therapy due to their implication in normal tissue toxicity from chronic inflammatory responses and mutagenesis. Gene expression can be used to determine abscopal effects at the molecular level. Synchrotron microbeam radiation therapy utilizing high-intensity X rays collimated into planar microbeams is a promising cancer treatment due to its reported ability to ablate tumors with less damage to normal tissues compared to conventional broadbeam radiation therapy techniques. The low scatter of synchrotron radiation enables microbeams to be delivered to tissue effectively, and is also advantageous for out-of-field studies because there is minimal interference from scatter. Mouse legs were irradiated at a dose rate of 49 Gy/s and skin samples in the out-of-field areas were collected. The out-of-field skin showed an increase in *Tnf* expression and a decrease in *Mdm2* expression, genes associated with inflammation and DNA damage. These expression effects from microbeam exposure were similar to those found with broadbeam exposure. In immune-deficient Ccl2 knockout mice, we identified a different gene expression profile which showed an early increase in *Mdm2*, *Tgfb1*, *Tnf* and *Ccl22* expression in out-of-field skin that was not observed in the immune-proficient mice. Our results suggest that the innate immune system is involved in out-of-field tissue responses and alterations in the immune response may not eliminate abscopal effects, but could change them.

INTRODUCTION

Radiation therapy is one of the main targeted treatment strategies for cancer control. Approximately 50% of all cancer patients receive radiation therapy as part of their treatment (*1*). One aspect of radiation therapy is that damage can occur in cells and tissue not directly hit by radiation, referred to as non-targeted effects. Not only are non-targeted effects found in the environment near the irradiated cells (''radiation-induced bystander effect'', RIBE), but these effects can occur at distant sites manifesting as the ''radiation-induced abscopal effect'' (RIAE) (*2–4*). RIBE mechanisms are relatively well characterized *in vitro* and *in vivo* (*5, 6*), but RIAE mechanisms which are complicated by systemic influences, complex tissue and cellular environments, are still not well understood. In addition, multiple signal transduction pathways are probably involved in RIAE (*7*). Early published studies demonstrated that tumors could be induced in nonirradiated animals with plasma from irradiated rats (*8*), and chromosomal damage could be induced in lymphocytes with plasma from irradiated patients (*9*). RIAE is implicated in induction of out-of-field normal tissue toxicity, including secondary cancers (*10, 11*). It has been suggested that radiation therapy outcomes could be improved by inhibiting non-targeted effects and reducing the possibility of secondary cancers (*12, 13*), which would be particularly advantageous in children (*12*). However, RIAE can also be advantageous for reducing distant out-of-field tumors (*14*).

It has been hypothesized that the immune system plays an important role in mediation of RIAE, in part through signal transduction (*3, 15*). Molecules associated with the cellular response to radiation include both p53-responsive and immunomodulatory factors (*16–18*). Little is known about the expression levels of these factors in tissues distant from the irradiated zone. Factors of particular interest include chemokine (C-C motif) ligand 2 (CCL2), also referred to as monocyte chemoattractant protein 1 (MCP1), which is known to recruit a number of immune cells, including memory T cells, monocytes and macrophages, to sites of

Editor's note. The online version of this article (DOI: https://doi.org/10.1667/RADE-19-00014.1) contains supplementary information that is available to all authorized users.

[1] Address for correspondence: School of Science, RMIT University, 124 La Trobe Street, Melbourne, Victoria, 3000 Australia; email: helen.forrester@rmit.edu.au.

[2] These authors contributed equally to this work.

tissue injury (*19*). The induction of reactive oxygen and nitrogen species (ROS and RNS) is important for this effect and can result in alteration of gene expression, DNA damage, genome instability and mutagenesis (*5*). In the grafted nonirradiated tumor model, CCL2 plasma levels were high, and there was tumor-induced DNA damage in the wild-type (WT) mice. However, a mouse knockout (KO) model of CCL2 did not show DNA damage in tissue distant from the tumor, implicating this cytokine as an important factor in the abscopal effect (*20*). C-C motif chemokine 22 (CCL22), also known as macrophage-derived chemokine (MDC), is another important cytokine, which activates chemotactic activity involving the attraction of monocytes, natural killer cells and dendritic cells, and activates T lymphocytes. The plasma level of this cytokine is induced with infection or injuries, including radiation-induced injuries, and is associated with RIAE (*21*). Other chemokines, such as C-C motif chemokine 11 (CCL11) attracts eosinophils, another immune cell type that stimulates the release of ROS and RNS that can also lead to oxidative stress and DNA damage (*22*). Transforming growth factor beta (TGF-β) is also of interest as it is involved in many cellular processes, including those in the response to radiation, involvement in tumorigenesis, and anti-tumor immune responses (*23*). TGF-β can act through the SMAD signaling pathway, which induces a set of transcription factors and has a complex regulation (*24*). Previously published studies have demonstrated RIAE in the form of tumor regression or reduced growth rate (*23, 25–29*), cellular or DNA damage (*21, 30–32*), or gene expression levels of out-of-field tissue after low-dose-rate broadbeam exposure (*33*). These studies have indicated that the immune system is involved in the observed RIAE (*21, 25, 27, 29*), or more specifically, through the NF-kappa B pathway (*33*), p53 (*28, 31*) or TGF-β (*23*).

Radiation therapy is an effective cancer treatment, but has the potential for improvement through the use of novel configurations including alteration of physical and spatial factors. Microbeam radiation therapy (MRT) is a promising preclinical radiotherapy technique that effectively ablates tumors and is relatively well tolerated by normal tissues in animal models (*37–41*). MRT utilizes high-intensity synchrotron-generated X rays spatially fractionated into planar microbeams with various dimensions. In the current study, 25-μm-wide beams were spaced 200 μm apart. The underlying mechanisms pertaining to MRT advantages are currently under investigation. Due to the defined geometry of the synchrotron X-ray beam and its low scatter, both MRT and broadbeam modes of synchrotron radiation are convenient experimental tools to conduct studies on out-of-field effects of radiation. In previously published studies, abscopal effects from synchrotron radiation, including MRT, were examined by analysis of clonogenic survival and calcium signaling potential (*34–36*). The use of both MRT and broadbeam configurations may provide insight into the mechanisms of MRT and how abscopal effects compare between the two modalities.

Here, we report changes in gene expression in mice locally irradiated on their hind leg with synchrotron MRT or conventional broadbeam configurations. We investigated the influence of irradiated target size, dose and beam modality on gene expression in the irradiated area and in out-of-field skin samples to better elucidate the factors involved in the induction and propagation of RIAE incurred by synchrotron radiation. We also compared the out-of-field tissue effects in C57BL/6 WT mice and immune-deficient Ccl2 KO mice, thus revealing a role of the signal transduction mediator, Ccl2, in RIAE. In this study, we examined levels of gene expression in the out-of-field tissue, and plasma cytokines. In parallel studies, performed utilizing the same mice, DNA damage, immune cell infiltration in distant tissues and additional plasma cytokines were analyzed (*30, 42*).

MATERIALS AND METHODS

Mice

Ethics approval for this study was obtained from the Monash University Animal Ethics Committee (approval no. MMCA/2012/01) and the Australian Synchrotron Animal Ethics Committee (approval no. AS-2012-01). Six-week-old C57BL/6 female mice were purchased from the Monash animal research platform and housed at the Australian Synchrotron (both in Clayton, Australia). Animals were monitored by members of the Monash animal research platform and given standard chow and Milli-Q® water. Immune-deficient Ccl2 KO mice on the C57BL/6J background were purchased from Jackson Laboratory (Bar Harbor, ME).

Irradiation and Tissue Collection

Just prior to irradiation, the mice were anesthetized with an intraperitoneal injection of 0.01 ml anesthesia mix per 1 g mouse weight from a stock made of 1 ml (100 mg/ml) ketamine, 0.1 ml xylazine (100 mg/ml) and 8.9 ml phosphate buffered saline (PBS). The right hind legs of the mice were shaved and the anesthetized mice were mounted on a custom jig that allowed the right hind leg to be irradiated as described elsewhere (*27*). Mice were irradiated at a dose rate of 49 Gy/s for 203 ms (10 Gy) or 810 ms (40 Gy) in an area of 8×8 mm^2 [or 2×2 mm^2; Supplementary Information (https://doi.org/10.1667/RADE-19-00014.1.S1)] on the right hind leg with an X-ray beam generated by the Australian Synchrotron at the Imaging and Medical Beam Line operating with a constant current of 200 mA. For MRT a collimator produced beam widths of 25 μm and microbeam center-to-center spaces of 200 μm.

Prior to irradiation, the site was marked and dose and location were confirmed with Gafchromic™ films EBT3 (dose range 1 cGy–40 Gy) and XRQA2 (dose range 1 mGy–20 cGy) (Ashland Inc., Bridgewater, NJ) taped to the outside of the leg. Control mice ($n = 25$) control mice received sham irradiation (0 Gy). In the initial experiment, skin samples from the backs of five C57BL/6 mice were collected 24 h after sham irradiation. In the subsequent experiment, tissue from 10 C57BL/6 and 10 Ccl2 KO mice were collected 72 and 144 h after sham irradiation (five mice in each group).

Dosimetry studies, presented elsewhere (*30, 42, 43*), indicated that 203 ms of MRT (''10 Gy'') resulted in a peak dose of approximately 7.5 Gy (dose rate of 37 Gy/s) and valley dose of approximately 0.094 Gy (dose rate of 0.5 Gy/s). Likewise, with MRT for 810 ms (''40 Gy''), peak dose was approximately 30 Gy and valley dose was

approximately 0.38 Gy. The integrated dose for 10 and 40 Gy MRT was approximately 1.2 and 4.6 Gy, respectively. The peak-to-valley dose ratio (PVDR) was approximately 80 ± 12 for an area of 8 × 8 mm^2 of 10 Gy MRT.

Whole skin samples from C57BL/6 mice were collected 24 and 96 h postirradiation in the initial experiment; and for the subsequent experiment, samples from C57BL/6 and Ccl2 KO mice were collected at 24, 72 and 144 h (five mice in each group). Each skin sample was taken from an out-of-field region (not irradiated) located approximately 35 mm from the irradiated site on the back of the mice. It was estimated that skin samples collected 35 mm from the irradiated site receiving a dose rate of 49 Gy/s for 203 ms would receive ultra-low doses of approximately 7.0 mGy and 0.8 mGy for broadbeam and MRT, respectively. After a dose rate of 49 Gy/s for 810 ms the same out-of-field skin site would receive 27.9 mGy and 3.26 mGy for broadbeam and MRT, respectively (*43*). Irradiated skin was also taken from the outside of the right hind leg using ink marks for orientation. The samples were immediately frozen on dry ice in cryovials and stored at –80°C.

RNA Isolation Procedure

RNA was extracted from the skin (epidermis and dermis layers) using RNeasy Fibrous Tissue Kit (QIAGEN, Hilden, Germany). The skin tissue samples were suspended in 0.3 ml of RLT buffer (QIAGEN) containing 10 µl of beta-mercaptoethanol (Sigma-Aldrich, Darmstadt, Germany) per 1 ml of RLT buffer, homogenized with a Precellys® homogenizer using 2.8-mm ceramic beads, sheared with 18g needle, added to 0.6 ml of water containing proteinase K and incubated at 55°C for 10 min. Tissue debris was removed by centrifugation for 3 min at 10,000*g* and the supernatant was collected. The RNA was precipitated with 100% ethanol and further purified on an RNeasy column (Qiagen, Venlo, Netherlands) using the RNAeasy method as per manufacturer's recommendation with the addition of a DNase1 digestion step. RNA concentration was determined using a NanoDrop ND-1000 spectrophotometer (Thermo Scientific™, Wilmington, DE).

Transcriptional Validation

Primers were designed to candidate exons or genes using ''primer 3'' or Primer-BLAST on-line software (National Center for Biotechnology Information, Bethesda, MD) (Supplementary Table S1; https://doi.org/10.1667/RADE-19-00014.1.S1). cDNA was made from 500 ng RNA using SuperScript® III First-Strand Synthesis System for RT-PCR (Invitrogen™, Carlsbad, CA) according to manufacturer's recommendations and as described elsewhere (*44, 45*). Real-time PCR was performed using these primers under the following conditions: SYBR® Green Master Mix (Applied Biosystems, UK) with 200 n*M* of each primer was mixed with 5 ng of cDNA. The cycling steps were as follows: 95°C for 10 min; (95°C for 15 s; 60°C for 60 s) × 40, with a melting temperature ramp following amplification. A robotic system was used to load a 384-well plate, which was then run on the ABI 7900 quantitative real time PCR machine. All samples were tested in triplicate. The expression levels [2^(reference CT-sample CT)] were calculated relative to the housekeeping gene 18s ribosomal RNA (Qm18s primers). The individual values for the RT-PCR experiment were multiplied by the same factor to give an average of 1 for the associated control. The control samples were collected at different times after sham irradiation for both mouse types. Although there was no significant difference between the gene expressions for different times after sham irradiation for either mouse types (data not shown), the corresponding time points (24, 72 or 144 h) were used for comparison in the qPCR. The expression results are the average of three separate PCR runs. Change in expression after irradiation was determined by comparing the relative gene expression of the skin from irradiated mice with the skin of nonirradiated mice collected at the corresponding locations. This included the cytokines, *Tgfb1*, *Ccl22*, *Ccl2* and *Tnf*, and DNA damage-responsive genes *Trp53* and *Mdm2*.

Plasma Cytokine Measurement

Blood samples were obtained by cardiac puncture and placed in ethylenediaminetetraacetic acid (EDTA)-containing tubes (Sarstedt AG & Co., Nümbrecht, Germany), centrifuged at 2,000 rpm for 10 min and then at 4,000 rpm for 10 min. The upper 90% of the plasma (total up to 200 µl) was transferred into 2-ml cryovials and stored at –80°C. Cytokines (TGF-β1, MDC/CCL22) in the 200-µl plasma samples were measured at RayBiotech Inc. (Norcross, GA) using the Quantibody® custom platform (a glass-chip-based multiplexed sandwich ELISA array) as described elsewhere (*42*). Control mouse plasma was collected from C57BL/6 and Ccl2 KO mice at 72 h after sham irradiation (five mice in each experimental group). Plasma from C57BL/6 mice were collected at 72 and 144 h postirradiation, and from Ccl2 KO mice at 24, 72 and 144 h postirradiation (five mice in each experimental group).

Statistical Analysis

Two-way analysis of variance (ANOVA) was used to analyze differences between doses, areas, radiation modalities and mouse strains. A two-tailed, unpaired Student's *t* test was used to determine the differences between irradiated and sham-irradiated skin. A *P* value of less than 0.05 was considered statistically significant.

RESULTS

Gene Expression Changes in Out-of-field Skin

A challenge with studying RIAE in animal models is the scatter radiation that causes low-dose irradiation to distant tissue. The advantage of using synchrotron radiation with a low energy and high dose rate (49 Gy/s) is the inherent low amount of scatter radiation (*42*). Cell signaling due to abscopal effect can cause gene expression changes in the tissue and can be used to monitor abscopal effect (*46*). We selected genes that have previously been associated with RIAE, such as tumor protein p53 (*Trp53*) (*28*, *31*) and transforming growth factor beta 1 (*Tgfb1*) (*23*), as well as a gene that would indicate DNA damage such as mouse double minute 2 (*Mdm2*) homolog (*16, 47*). We also included genes that indicate an inflammatory response and/or activation of macrophages such as tumor necrosis factor (*Tnf*) (*48*), C-C motif chemokine ligand 22 (*Ccl22*) (*21*) and Ccl2 (*19*, *20*). A skin area of 8 × 8 mm^2 was irradiated on the mouse's leg and RNA was extracted from out-of-field skin collected from the mouse's back, approximately 35 mm from the site of irradiation. Gene expression changes that occurred in out-of-field skin samples are shown in Fig. 1. Samples from control mice were collected at 24 h after sham irradiation. Gene expression levels of *Tnf* and *Tgfb1* increased in the out-of-field skin. The increase in *Tnf* gene expression was significant 24 h after 40 Gy MRT ($P = 0.037$). The increase in *Tgfb1* gene expression was significant 96 h after 10 Gy MRT ($P = 0.035$). *Ccl22* expression levels decreased 24 h after 10 Gy broadbeam exposure ($P = 0.024$) and 96 h after 10 Gy MRT ($P = 0.047$). This indicates a systemic inflammatory response.

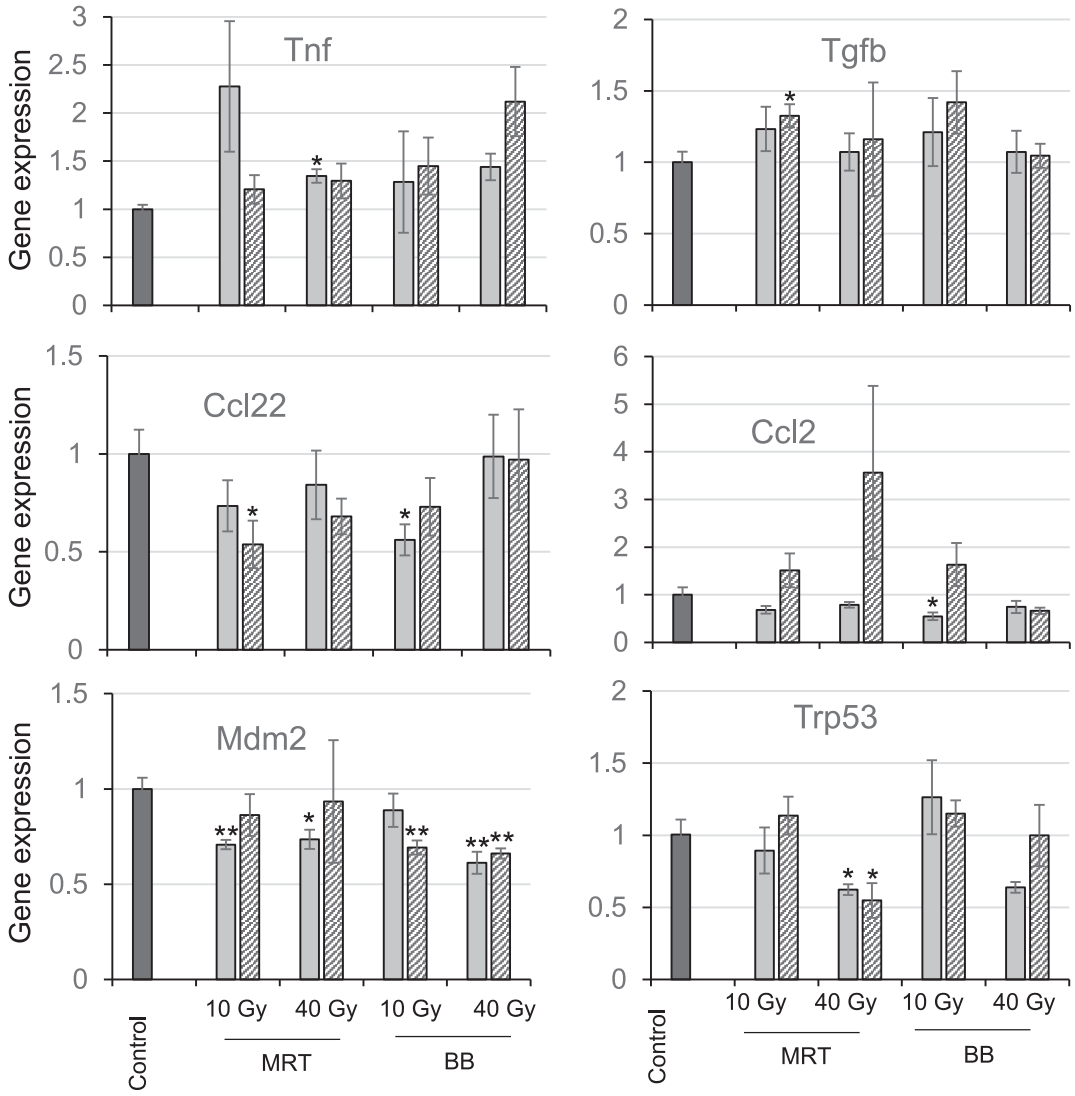

FIG. 1. Differential gene expression in out-of-field skin of C57BL/6 mice after broadbeam exposure or MRT. Relative gene expression levels were determined using qRT-PCR of RNA isolated from mouse skin at 24 h (solid) and 96 h (patterned) after 10 or 40 Gy broadbeam exposure and MRT from out-of-field skin for the inflammatory genes *Tgfb1*, *Ccl22*, *Tnf and Ccl2*, and stress-related genes *Mdm2* and *Trp53*. Controls were from samples collected 24 h after sham irradiation (black). Significant differences compared to controls are indicated at $*P < 0.05$ and $**P < 0.01$. n $\geq$ 4. Error bars represent SEM.

In the out-of-field skin there was a decrease in *Ccl2*, *Mdm2* and *Trp53* gene expression. There was a statistically significant decrease in *Ccl2* expression levels at 24 h after 10 Gy broadbeam exposure ($P = 0.037$). This decrease in *Ccl2* expression levels was not present 96 h postirradiation. *Mdm2* expression levels decreased 24 h after 10 Gy MRT ($P = 0.003$), 40 Gy MRT ($P = 0.016$) and 40 Gy broadbeam exposure ($P = 0.003$), and at 96 h after 40 Gy broadbeam ($P = 0.01$) and 10 Gy broadbeam ($P = 0.004$) irradiation. The decrease in *Mdm2* expression levels correspond with a decrease in *Trp53* gene expression levels at 24 h ($P = 0.046$) and 96 h ($P = 0.046$) after 40 Gy MRT.

The level of modulation was similar for the different modalities, MRT and broadbeam exposure. However, there was a statistically significant difference between 10 and 40 Gy at 24 h postirradiation with a greater decrease in *Trp53* gene expressions in out-of-field skin for MRT and broadbeam ($P = 0.0069$ and 0.0063, respectively). Similar results were observed when a smaller area of skin (2×2 mm^2) was irradiated (Supplementary Fig S1; https://doi.org/10.1667/RADE-19-00014.1.S1), indicating that the observed abscopal changes are also independent of the irradiated region size. Corresponding skin samples at the site of irradiation were also analyzed (Supplementary Fig. S2; https://doi.org/10.1667/RADE-19-00014.1.S1) to demonstrate the similarities and differences with out-of-field tissues. The expression of cytokine genes *Tnf*, *Tgfb1* and *Ccl22* increased, indicating an ongoing inflammatory response at the site of irradiation.

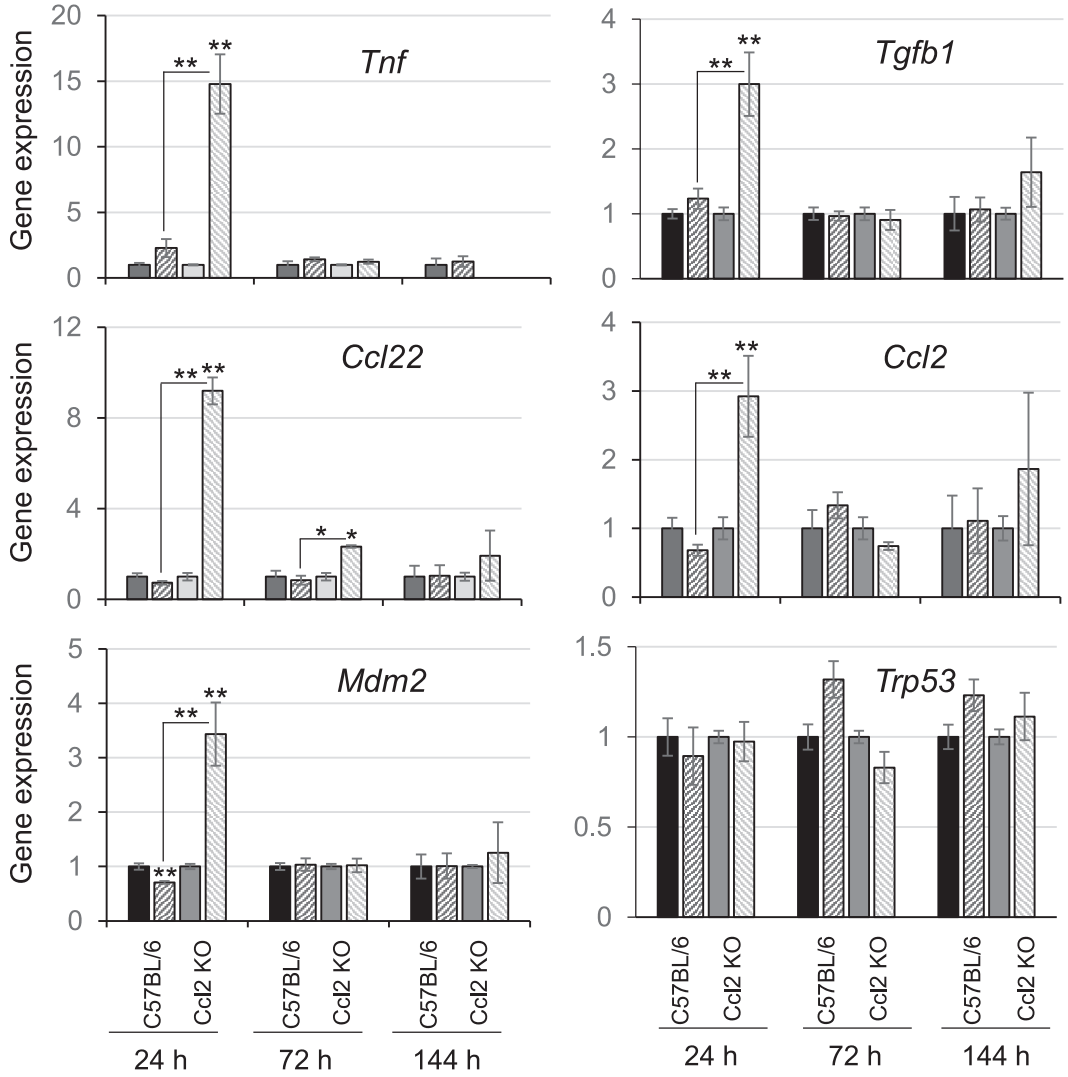

FIG. 2. Differential gene expression in out-of-field skin after 10 Gy MRT in immune-deficient Ccl2 KO and C57BL/6 WT mice. Relative gene expression levels were determined using qRT-PCR of RNA isolated from mouse skin at 24, 72 and 144 h after 10 Gy MRT in C57BL/6 mice (black patterned) or Ccl2 KO mice (gray patterned) compared to relevant sham-irradiated control (solid black for C57BL/6 mice and solid gray for Ccl2 KO mice) for the inflammatory genes *Tnf*, *Tgfb1*, *Ccl22*, *Ccl2*, *Mdm2* and *Trp53*. Control samples were collected 24, 72 or 144 h after sham irradiation and the relevant controls used are represented in the bar graph next to the gene expression of the irradiated samples. Asterisks (*) indicate significant differences compared to the time-appropriate sham-irradiated controls (24, 72, and 144 h after sham irradiation) and asterisks above a line indicate significant differences between the C57BL/6 and Ccl2 KO mice (*$P < 0.05$ and **$P < 0.01$). n $\geq$ 4. Error bars represent SEM.

Ccl2 KO Mice

Previously published studies implicated the CCL2 cytokine as an important factor in the tumor-induced abscopal effect by demonstrating that Ccl2 KO mice do not show DNA damage in tissue distant from the tumor, whereas the presence of the tumor-induced DNA damage in the WT mice (*20*). To study the effects of CCL2 on radiation-induced abscopal effects, we irradiated Ccl2 KO mice and compared them to the C57BL/6 WT mice. In a parallel study (*42*), abscopal DSB, oxidative DNA damage and apoptosis were inhibited in Ccl2 KO mice, while present in C57BL/6 WT mice. Here we found that in the out-of-field skin of Ccl2 KO mice there was a dramatic increase in expression levels of *Tnf*, *Tgfb*, *Ccl22*, *Ccl2 and Mdm2* at 24 h after 10 Gy MRT compared to the control mice (Fig. 2). The increase in *Tnf* expression of approximately 15-fold ($P = 0.0005$) was significantly different from the increase detected in the out-of-field skin of the C57BL/6 WT mice 24 h postirradiation ($P = 0.003$); but at 72 h postirradiation, the *Tnf* expression levels were similar to the expression levels in C57BL/6 mice. Similar to the data found in the immunocompetent mice, the *Tgfb1* expression increased approximately threefold ($P = 0.006$) in the Ccl2 KO mice 24 h postirradiation. This increase in *Tgfb1* expression was significantly higher in the Ccl2 KO mice

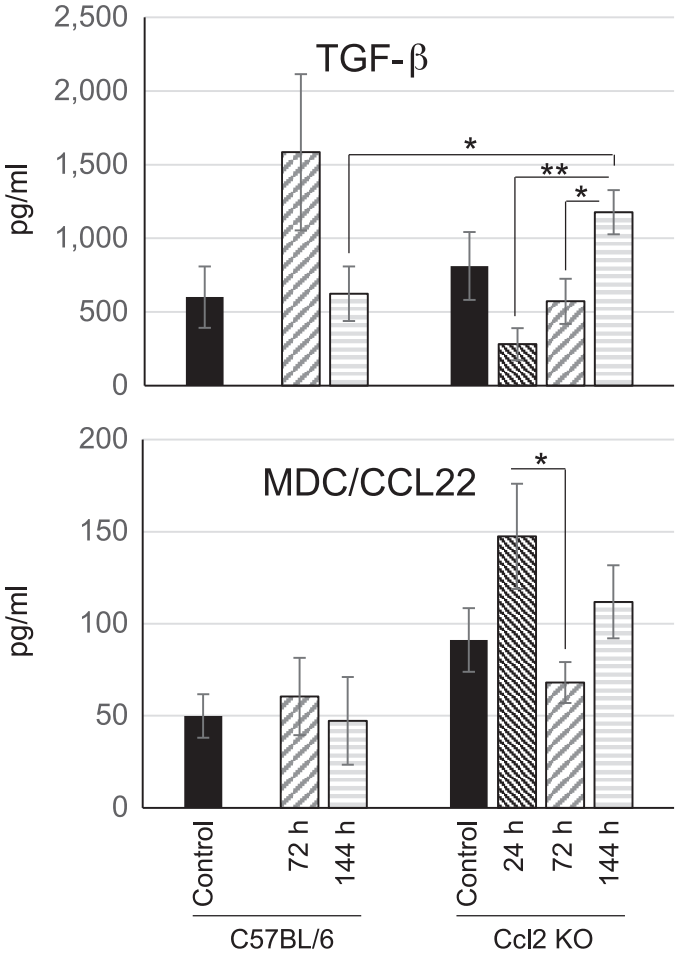

FIG. 3. Plasma cytokine levels after 10 Gy MRT in immune-deficient Ccl2 KO and C57BL/6 WT mice. TGF-β and MDC/CCL22 protein levels in the plasma from mouse skin in control mice (black) at 24 (black patterned; Ccl2 KO only), 72 (gray patterned) and 144 h (gray horizontal lines) after 10 Gy MRT in C57BL/6 mice or Ccl2 KO mice. Asterisks (*) indicate significant differences compared to sham irradiated controls (72 h after sham irradiation) and asterisks above a line indicate significant differences between the C57BL/6 and Ccl2 KO mice (*$P < 0.05$ and **$P < 0.01$). n $\geq$ 4. Error bars represent SEM.

compared with the C57BL/6 mice ($P = 0.0043$). This is associated with a corresponding increase in TGF-β in the plasma of Ccl2 KO mice (Fig. 3) where there is a significant increase in TGF-β between 24 h and 144 h ($P = 0.0029$). Furthermore, there is significantly more TGF-β protein in the plasma of Ccl2 KO mice compared to the C57BL/6 immunocompetent mice at 144 h postirradiation ($P = 0.049$) (Fig. 3).

Ccl22 expression increased approximately ninefold in the out-of-field skin of Ccl2 KO mice 24 h postirradiation ($P = 0.002$) and there was still approximately a twofold increase at 72 h postirradiation ($P = 0.036$). This was higher than the expression level detected in the C57BL/6 mice at both 24 h ($P = 0.0021$) and 72 h ($P = 0.0182$) postirradiation. However, no significant increase in MDC/CCL22 protein levels was detected in the plasma of the Ccl2 KO mice (Fig. 3). There was a decrease in MDC/CCL22 plasma protein from 24 h to 72h in the Ccl2 KO mice.

Although the Ccl2 KO mouse does not produce the functional MCP-1 protein, it does produce an altered *Ccl2* mRNA (*49*), which enabled the measurement of transcription expression levels of *Ccl2* in the Ccl2 KO mouse. There was an approximately threefold increase in *Ccl2* expression in the out-of-field skin from Ccl2 KO mice 24 h after 10 Gy MRT ($P = 0.004$), which was significantly different from the levels for the out-of-field skin from the C57BL/6 mice ($P = 0.0006$) where no increase was detected. An increase in *Ccl2* transcripts for the out-of-field skin of the Ccl2 KO mice 24 h postirradiation suggests an attempt to provide a functional CCL2 protein due to a lack of required functional protein.

The change in *Mdm2* expression level in the out-of-field skin for the Ccl2 KO mice increased more than threefold ($P = 0.003$). This was significantly different from the C57BL/6 mice ($P = 0.0005$), which had a decrease in the *Mdm2* expression level 24 h postirradiation. There was no significant difference in the *Trp53* gene expression in the out-of-field skin of the mice. In the targeted skin that received 10 Gy MRT, there was no expression difference between Ccl2 KO mice and C57BL/6 mice for *Tnf*, *Tgfb*, *Ccl22*, *Ccl2* or *Trp53* (Supplementary Fig. S3; https://doi.org/10.1667/RADE-19-00014.1.S1). However, the amount of change in *Mdm2* gene expression was different between the irradiated skin of Ccl2 KO mice and the C57BL/6 mice at 24 and 72 h postirradiation ($P = 0.0245$ and 0.0396, respectively). The dramatic increases in gene expression levels of the out-of-field skin of Ccl2 KO mice did not occur in the irradiated skin.

DISCUSSION

To our knowledge, this is the first published study in which gene expression levels in out-of-field skin are compared between immune-deficient Ccl2 KO mice with C57BL/6 WT mice using synchrotron radiation. We have also demonstrated that gene expression is a useful tool to examine radiation-induced abscopal effects. In this study, six key genes were selected which included genes implicated in RIAE, *Tgfb* (*23*) and *Tp53* (*28, 31*), an indicator of M1 macrophage activation, *Tnf* (*48*), immune cell attractants, *Ccl2* (*19*) and *Ccl22* (*21*), and an indicator of DNA damage and stress, *Mdm2* (*16, 47*). We detected gene expression changes for all six of these genes in out-of-field skin 24 h after MRT and broadbeam exposure in C57BL/6 mice, and all showed a degree of independence from dose and radiation modality. In previously published work, we noted many differences in gene expression levels in targeted tumors between MRT and broadbeam modalities, but interestingly, even though *Mdm2* expression levels increased after irradiation there was no difference in the level between the modalities (*17*).

Mouse skin is a complex organ consisting of various layers and cell types: a surface epithelium (epidermis), a connective tissue layer (dermis), an adipose tissue layer (hypodermis), as well as hair follicles and blood vessels. The RNA was obtained from the epidermis and dermis layers. Therefore, the types of cells responsible for the gene expression changes within the skin were not identified. In addition, changes to the gene expression could be a result of an increase or decrease in infiltrating cells or activation of immune cells within the skin. In our parallel studies utilizing the same mice as used in this study, increases in DNA damage were detected in the out-of-field duodenum but not in the skin epidermis of C57BL/6 mice (*30, 42*). Similar to the gene expression findings, the systemic genotoxic events, namely oxidative stress, complex DNA damage and apoptosis, were induced at comparable levels in out-of-field tissues of C57BL/6 mice irradiated with various doses for both radiation modalities, MRT and broadbeam (*30*).

We were interested in the gene expression of *Ccl2* due to its possible involvement in abscopal effects (*20*) since it is known to attract monocytes (*19*). Aravindan *et al*. detected activation of the NFκB pathway in out-of-field heart tissue of C57BL/6 mice 24 h after 2 Gy and 10 Gy broadbeam exposure of the lower abdomen, and used a panel of 88 NFκB signaling pathway genes, which included both *Ccl2* and *Tnf*, to detect gene expression changes (*33*). Similar to our findings, *Tnf* gene expression levels increased after receiving 2 Gy They also observed an increase in *Ccl2* after receiving both 2 Gy and 10 Gy, which was different from our findings. It is interesting to note that many of the genes with expression that increased after receiving both 2 Gy and 10 Gy, including Ccl2, also showed dose-independent upregulation. In contrast to this study, we found no significant change in *Ccl2* gene expression levels in the out-of-field skin of C57BL/6 mice after receiving either MRT or broadbeam, and a significant decrease 24 h after 10 Gy broadbeam exposure. The differences in observation of *Ccl2* gene responses could be due to variations in target (abdomen vs. leg) and/or out-of-field (heart vs. skin) tissue types. It is likely that RIAE elicit responses in a tissue-specific manner and probably involve variations in the resultant pathways towards producing abscopal end points (*7, 34*). Additionally, dose rate could be a factor; we used a dose rate of 49 Gy/s, whereas Aravindan *et al*. used a considerably lower dose rate of 0.81 Gy/min (*33*). The dose-rate influence is not without precedence, as there is evidence that dose rates influence RIAE (*7*). This could be an important aspect for synchrotron radiation therapy and warrants further investigation. Recently published studies indicate that the higher MRT doses (approximately 400 Gy peak dose compared to our 10 and 40 Gy peak dose) and broadbeam modalities induce different immunological responses in targeted tissue (*50, 51*) which may produce varied abscopal effects. This includes a higher level of CCL2 protein in the targeted tumor after broadbeam exposure compared to MRT (*51*).

Previously published studies have indicated that the immune system is involved in the observed RIAE (*21, 25, 27, 29*). Therefore, the presence of immune cells within the out-of-field tissue is important. Changes have been found in out-of-field skin epidermis and hair follicles after MRT and broadbeam exposure (*30*), with increases in frequencies of $F4/80^+$ macrophages, $Ly\text{-}6G^+$ neutrophils and $CD3^+$ T cells. Activation of these immune cells can increase the gene expression of *Tnf* (as seen 24 h after 40 Gy MRT), and indicates an inflammatory environment (*48*), which can cause cell damage and death (*52*). The DNA damage detected in RIAE has been attributed to ROS and RNS produced by activated M1 macrophages; however, M2 macrophages do not produce ROS and RNS (*53*). *Mdm2* gene expression level is an indicator of DNA damage and is induced by stress (*54*) and radiation (*16, 47*), but MDM2 protein is also implicated in the inflammatory process and may be involved in M2 macrophage polarization (*55*). An increase of *Mdm2* expression is associated with ubiquitination of p53 protein leading to a decrease in p53. This can result in an increase in cell survival due to limiting of the apoptotic effects of p53 and shortening of cell cycle arrest time (*56*). Downregulation of Mdm2 stabilizes p53 protein and results in increased apoptosis (*57*). Interestingly, abscopal tumor shrinkage is found to be absent in p53-null tumors in a mouse model, suggesting that p53 protein is important for anti-tumor RIAE (*58*). An increase of p53 also controls M2 macrophage polarization and results in a decrease in the anti-inflammatory M2 genes (*55*). In the current studies, we observed a decrease in *Mdm2* and an increase in *Tnf* in the out-of-field skin of the C57BL/6 mice 24 h postirradiation, indicating an environment that promotes the activation of ROS and RNS producing M1 macrophages. This may contribute to the increase in abscopal DNA damage detected in our parallel studies (*30, 42*).

In contrast to the C57BL/6 WT mice, there was a higher level of M2 macrophage-associated genes such as *Tgfb1*, *Ccl22* and *Mdm2* (*55, 59*) in the out-of-field skin of the Ccl2 KO mice 24 h postirradiation. Although Ccl2 KO mice lack functional CCL2 protein, which would normally recruit macrophages, the level of residential macrophages in these mice is similar to C57BL/6 WT mice (*49*). A significant increase in the TGF-β protein plasma level from 24 to 144 h postirradiation was consistent with the increase in *Tgfb1* expression level (Fig. 3). The TGF-β plasma levels were also higher in Ccl2 KO mice compared to the C57BL/6 WT mice at 144 h postirradiation. We could speculate that the high levels of TGF-β in the plasma at 144 h postirradiation may originate from out-of-field tissue rather than the site of irradiation, but the regulation of the protein expression is complex. TGF-β has an anti-inflammatory effect and inhibits T-cell-induced immunity effects in tumors (*23*), so differences in TGF-β plasma levels may influence RIAE.

The Ccl2 KO mice have a lower level of MDC/CCL22 plasma protein at 72 h compared to 24 h postirradiation, but neither plasma levels at 24 or 72 h are significantly higher than in the control animals. This was not consistent with the gene expression data where there was a significant increase in *Ccl22* expression levels at both 24 and 72 h postirradiation. There are a number of possible explanations for this, including that the sensitivity of gene expression may be better than protein expression, protein regulation downstream, or systemic transport may affect plasma MDC/CCL22. We hypothesize that there was an anti-inflammatory environment in the out-of-field skin of the Ccl2 KO mice, resulting in M2 macrophage polarization and a reduction of the M1/M2 macrophage ratio. Thus, the production of DNA-damaging ROS and RNS was lower in the Ccl2 KO mice compared to the C57BL/6 WT mice producing less DNA damage as observed in the parallel study (*42*). Generally, no significant increase in DNA base damage was detected in the tissue of Ccl2 KO mice with only a small increase detected in the tongue 144 h postirradiation (*42*). Additionally, an increase in γ-H2AX foci detected in the out-of-field duodenum of C57BL/6 WT mice was absent in the Ccl2 KO mice (*42*). However, the increase in *Tnf* gene expression levels in the out-of-field skin of the Ccl2 KO mice, which indicates an inflammatory environment, is in disagreement with the notion that there is an anti-inflammatory environment in the out-of-field skin. This suggests that it might not just be an increase in M2 macrophages but a problem with M1 polarization. TNF induces the *Ccl2* gene (*60*) and CCL2 protein is involved in M1 macrophage polarization (*61*). The lack of functional CCL2 protein in the Ccl2 KO mice may affect the M1 macrophage polarization that would normally occur due to radiation-induced abscopal effects.

In conclusion, gene expression has proved to be an effective means to detect RIAE from exceedingly low-scatter synchrotron radiation, and different signal transduction pathways were indicated. Future studies are required to determine which factors may be beneficial to inhibit, and which to enhance for improved cancer radiation therapy treatment. However, inhibition of factors such as CCL2 may change RIAE but may not eliminate all systemic effects. As the DNA damage in distant tissue has been attributed to ROS and RNS produced by M1 macrophages, the signal transduction pathways involved in polarization of M1 or M2 macrophages may provide a key to the control of RIAE.

SUPPLEMENTARY INFORMATION

Table S1. PCR primer sequences.

Fig. S1. Differential gene expression in out-of-field skin of C57BL/6 mice after broadbeam or MRT.

Fig. S2. Differential gene expression in targeted skin of C57BL/6 mice after broadbeam or MRT.

Fig. S3. Differential gene expression in targeted skin after 10 Gy MRT in immune-deficient Ccl2 KO and C57BL/6 WT mice.

ACKNOWLEDGMENTS

We thank Andrea Smith, Jessica Ventura, Jason Palazzolo and Alesia Ivashkevich for technical assistance. This work was supported by the Australian National Health and Medical Research Council (grant no. 10275598). Also, this project was supported through the 2010 round of the priority-driven Collaborative Cancer Research Scheme (grant no. 1002743) and funded by the Australian Government Department of Health and Ageing with the assistance of Cancer Australia. Also, support was provided by the Victorian Government's Operational Infrastructure Support Program. The funders had no role in study design, data collection and analysis, decision to publish or preparation of the manuscript.

Received: December 13, 2019; accepted: August 24, 2020; published online: September 29, 2020

REFERENCES

1. Delaney G, Jacob S, Featherstone C, Barton M. The role of radiotherapy in cancer treatment: estimating optimal utilization from a review of evidence-based clinical guidelines. Cancer 2005; 104:1129–37.
2. Formenti SC, Demaria S. Systemic effects of local radiotherapy. Lancet Oncol 2009; 10:718–26.
3. Shiraishi K, Nakagawa K, Niibe Y, Ishiwata Y, Yokochi S, Ohtomo K, et al. Abscopal effect of radiation therapy and signal transduction. Curr Signal Transduct Ther 2010; 5:212–22.
4. Siva S, Macmanus MP, Martin RF, Martin OA. Abscopal effects of radiation therapy: A clinical review for the radiobiologist. Cancer Lett 2015; 356:82–90.
5. Sprung CN, Ivashkevich A, Forrester HB, Redon CE, Georgakilas A, Martin OA. Oxidative DNA damage caused by inflammation may link to stress-induced non-targeted effects. Cancer Lett 2015; 356:72–81.
6. Hatzi VI, Laskaratou DA, Mavragani IV, Nikitaki Z, Mangelis A, Panayiodis MI, et al. Non-targeted radiation effects in vivo: A critical glance of the future in radiobiology. Cancer Lett 2015; 356:34–42.
7. Blyth BJ, Sykes PJ. Radiation-induced bystander effects: what are they, and how relevant are they to human radiation exposures? Radiat Res 2011; 176:139–57.
8. Suoto J. Tumour development in the rat induced by blood of irradiated animals. Nature 1962; 195:1317–8.
9. Hollowell JG, Littlefield LG. Chromosome damage induced by plasma of x-rayed patients: an indirect effect of x-ray. Proc Soc Exp Biol Med 1968; 129:240–4.
10. Bostrom PJ, Soloway MS. Secondary cancer after radiotherapy for prostate cancer: should we be more aware of the risk? Eur Urol 2007; 52:973–82.
11. Martin O, Martin RF. Cancer radiotherapy: Understanding the price of tumour eradication Front Cell Dev Biol 2020; 8:261.
12. Martin OA, Yin X, Forrester HB, Sprung CN, Martin RF. Potential strategies to ameliorate risk of radiotherapy-induced second malignant neoplasms. Semin Cancer Biol 2016; 37–8:65–76.
13. Cheki M, Yahyapour R, Farhood B, Rezaeyan A, Shabeeb D, Amini P, et al. COX-2 in radiotherapy: A potential target for radioprotection and radiosensitization. Curr Mol Pharmacol 2018; 11:173–83.
14. Ishiyama H, Teh BS, Ren H, Chiang S, Tann A, Blanco AI, et al. Spontaneous regression of thoracic metastases while progression of brain metastases after stereotactic radiosurgery and stereotactic body radiotherapy for metastatic renal cell carcinoma: abscopal

effect prevented by the blood-brain barrier? Clin Genitourin Cancer 2012; 10:196–8.

15. Calveley VL, Khan MA, Yeung IW, Vandyk J, Hill RP. Partial volume rat lung irradiation: temporal fluctuations of in-field and out-of-field DNA damage and inflammatory cytokines following irradiation. Int J Radiat Biol 2005; 81:887–99.
16. Sprung CN, Li J, Hovan D, McKay MJ, Forrester HB. Alternative transcript initiation and splicing as a response to DNA damage. PLoS One 2011; 6:e25758.
17. Sprung CN, Yang Y, Forrester HB, Li J, Zaitseva M, Cann L, et al. Genome-wide transcription responses to synchrotron microbeam radiotherapy. Radiat Res 2012; 178:249–59.
18. Sprung CN, Forrester HB, Siva S, Martin OA. Immunological markers that predict radiation toxicity. Cancer Lett 2015; 368:191–7.
19. Kurihara T, Warr G, Loy J, Bravo R. Defects in macrophage recruitment and host defense in mice lacking the CCR2 chemokine receptor. J Exp Med 1997; 186:1757–62.
20. Redon CE, Dickey JS, Nakamura AJ, Kareva IG, Naf D, Nowsheen S, et al. Tumors induce complex DNA damage in distant proliferative tissues in vivo. Proc Natl Acad Sci U S A 2010; 107:17992–7.
21. Siva S, Lobachevsky P, MacManus MP, Kron T, Moller A, Lobb RJ, et al. Radiotherapy for non-small cell lung cancer induces DNA damage response in both irradiated and out-of-field normal tissues. Clin Cancer Res 2016; 22:4817–26.
22. Parajuli B, Horiuchi H, Mizuno T, Takeuchi H, Suzumura A. CCL11 enhances excitotoxic neuronal death by producing reactive oxygen species in microglia. Glia 2015; 63:2274–84.
23. Vanpouille-Box C, Diamond JM, Pilones KA, Zavadil J, Babb JS, Formenti SC, et al. TGFbeta is a master regulator of radiation therapy-induced antitumor immunity. Cancer Res 2015; 75:2232–42.
24. Kamato D, Burch ML, Piva TJ, Rezaei, HB, Rostam, MA, Xu S, et al. Transforming growth factor-beta signalling: role and consequences of Smad linker region phosphorylation. Cell Signal 2013; 25:2017–24.
25. Ohba K, Omagari K, Nakamura T, Ikuno N, Saeki S, Matsuo I, et al. Abscopal regression of hepatocellular carcinoma after radiotherapy for bone metastasis. Gut 1998; 43:575–7.
26. Reynders K, Illidge T, Siva S, Chang JY, De Ruysscher D. The abscopal effect of local radiotherapy: using immunotherapy to make a rare event clinically relevant. Cancer Treat Rev 2015; 41:503–10.
27. Rodriguez-Ruiz ME, Vanpouille-Box C, Melero I, Formenti SC, Demaria S. Immunological mechanisms responsible for radiation-induced abscopal effect. Trends Immunol 2018; 39:644–55.
28. Camphausen K, Moses MA, Menard C, Sproull M, Beecken WD, Folkman J, et al. Radiation abscopal antitumor effect is mediated through p53. Cancer Res 2003; 63:1990–3.
29. Dewan MZ, Galloway AE, Kawashima N, Dewyngaert JK, Babb JS, Formenti SC, et al. Fractionated but not single-dose radiotherapy induces an immune-mediated abscopal effect when combined with anti-CTLA-4 antibody. Clin Cancer Res 2009; 15:5379–88.
30. Ventura J, Lobachevsky PN, Palazzolo JS, Forrester H, Haynes NM, Ivashkevich A, et al. Localized synchrotron irradiation of mouse skin induces persistent systemic genotoxic and immune responses. Cancer Res 2017; 77:6389–99.
31. Lorimore SA, Rastogi S, Mukherjee D, Coates PJ, Wright EG. The influence of p53 functions on radiation-induced inflammatory bystander-type signaling in murine bone marrow. Radiat Res 2013; 179:406–15.
32. Mohye El-Din AA, Abdelrazzak AB, Ahmed MT, El-Missiry MA. Radiation induced bystander effects in the spleen of cranially-irradiated rats. Br J Radiol 2017; 90:20170278.
33. Aravindan S, Natarajan M, Ramraj SK, Pandian V, Khan FH, Herman TS, et al. Abscopal effect of low-LET gamma-radiation mediated through Rel protein signal transduction in a mouse model of nontargeted radiation response. Cancer Gene Ther 2014; 21:54–9.
34. Fernandez-Palomo C, Schultke E, Smith R, Brauer-Krisch E, Laissue J, Schroll C, et al. Bystander effects in tumor-free and tumor-bearing rat brains following irradiation by synchrotron X-rays. Int J Radiat Biol 2013; 12:72–92.
35. Fernandez-Palomo C, Brauer-Krisch E, Laissue J, Vukmirovic D, Blattmann H, Seymour C, et al. Use of synchrotron medical microbeam irradiation to investigate radiation-induced bystander and abscopal effects in vivo. Physica Medica 2015; 31:584–95.
36. Fernandez-Palomo C, Schultke E, Brauer-Krisch E, Laissue JA, Blattmann H, Seymour C, et al. Investigation of abscopal and bystander effects in immunocompromised mice after exposure to pencilbeam and microbeam synchrotron radiation. Health Phys 2016; 111;149–59.
37. Brauer-Krisch E, Serduc R, Siegbahn EA, Le Duc G, Prezado Y, Bravin, et al. Effects of pulsed, spatially fractionated, microscopic synchrotron X-ray beams on normal and tumoral brain tissue. Mutat Res 2010; 704:160–6.
38. Dilmanian FA, Morris GM, Zhong N, Bacarian T, Hainfiels JF, Kalef-Ezra J, et al. Murine EMT-6 carcinoma: high therapeutic efficacy of microbeam radiation therapy. Radiat Res 2003; 159:632–41.
39. Laissue JA, Geiser G, Spanne PO, Dilmanian FA, Gebbers JO, Geiser, M, et al. Neuropathology of ablation of rat gliosarcomas and contiguous brain tissues using a microplanar beam of synchrotron-wiggler-generated X rays. Int J Cancer 1998; 78:654–60.
40. Slatkin DN, Spanne P, Dilmanian FA, Gebbers JO, Laissue JA. Subacute neuropathological effects of microplanar beams of x-rays from a synchrotron wiggler. Proc Natl Acad Sci U S A 1995; 92:8783–7.
41. Fernandez-Palomo C, Fazzari J, Trappetti V, Smyth L, Janka H, Laissue J, et al. Animal models in microbeam radiation therapy: A scoping review. Cancers (Basel) 2020; 12:527.
42. Lobachevsky PN, Ventura J, Giannakandropoulou L, Forrester H, Palazzolo JS, Haynes NM, et al. A functional immune system is required for the systemic genotoxic effects of localised irradiation. Int J Radiat Oncol Biol Phys 2019; 103:1184–93.
43. Lobachevsky P, Ivashkevich A, Forrester HB, Stevenson AW, Hall CJ, Sprung CN, et al. Assessment and implications of scattered microbeam and broadbeam synchrotron radiation for bystander effect studies. Radiat Res 2015; 184:650–9.
44. Forrester HB, Ivashkevich A, McKay MJ, Leong T, de Krester DM, Sprung CN. Follistatin is induced by ionizing radiation and potentially predictive of radiosensitivity in radiation-induced fibrosis patient derived fibroblasts. PLoS One 2013; 8:e77119.
45. Forrester HB, Sprung CN. Intragenic controls utilizing radiation-induced alternative transcript regions improves gene expression biodosimetry. Radiat Res 2014; 181:314–23.
46. Sokolav M, Neumann R. Changes in gene expression as one of the key mechanisma involved in radiation-induced bystander effects (review). Biomed Reports 2018; 9:99–111.
47. Perry ME. Mdm2 in the response to radiation. Mol Cancer Res 2004; 2:9–19.
48. Stout RD. Macrophage activation by T cells: cognate and non-cognate signals. Curr Opin Immunol 1993; 5:398–403.
49. Lu B, Rutledge BJ, Gu L, Fiorillo J, Lukacs, NW, Kunkel SL, et al. Abnormalities in monocyte recruitment and cytokine expression in monocyte chemoattractant protein 1-deficient mice. J Exp Med 1998; 187:601–8.
50. Potez M, Fernandez-Palomo C, Bouchet A, Trappetti V, Donzelli M, Krisch M, et al. Synchrotron microbeam radiation therapy as a new approach for the treatment of radioresistant melanoma: potential underlying mechanisms. Int J Radiat Oncol Biol Phys 2019; 105:1126–36.

51. Yang Y, Swierczak A, Ibahim M, Paiva P, Cann L, Stevenson AW, et al. Synchrotron microbeam radiotherapy evokes a different early tumor immunomodulatory response to radiotherapy in EMT6.5 mammary tumors. Radiother Oncol 2019; 133:93–9.

52. Fehsel K, Kolb-Bachofen V, Kolb H. Analysis of TNF alpha-induced DNA strand breaks at the single cell level. Am J Pathol 1991; 139:251–4.

53. Mantovani A, Biswas SK, Galdiero MR, Sica A, Locati M. Macrophage plasticity and polarization in tissue repair and remodelling. J Pathol 2013; 229:176–85.

54. Chandler DS, Singh RK, Caldwell LC, Bitler JL, Lozano G. Genotoxic stress induces coordinately regulated alternative splicing of the p53 modulators MDM2 and MDM4. Cancer Res 2006; 66:9502–8.

55. Li L, Ng DSW, Mah W-C, Almeida FF, Rahmat SA, Rao VK, et al.. A unique role for p53 in the regulation of M2 macrophage polarization. Cell Death Differ 2015; 22:1081–93.

56. Ewen ME, Miller SJ. p53 and translational control. Biochim Biophys Acta 1996; 1242:181–4.

57. Inoue T, Geyer RK, Yu ZK, Maki CG. Downregulation of MDM2 stabilizes p53 by inhibiting p53 ubiquitination in response to specific alkylating agents. FEBS Lett 2001; 490:196–201.

58. Strigari L, Mancuso M, Ubertini V, Soriani A, Giardullo P, Benassi M, et al. Abscopal effect of radiation therapy: Interplay between radiation dose and p53 status. Int J Radiat Biol 2014; 90:248–55.

59. Atri C, Guerfali FZ, Laouini D. Role of human macrophage polarization in inflammation during infectious diseases. Int J Mol Sci 2018; 19:1801.

60. Loupasakis K, Kuo D, Sokhi UK, Sohn C, Syracuse B, Glannopoulou EG, et al. Tumor necrosis factor dynamically regulates the mRNA stabilome in rheumatoid arthritis fibroblast - like synoviocytes. PLoS One 2017; 12:e0179762.

61. Carson WF, Salter-Green SE, Scola MM, Joshi A, Gallagher KA, Kunkel SL. Enhancement of macrophage inflammatory responses by CCL2 is correlated with increased miR-9 expression and downregulation of the ERK1/2 phosphatase Dusp6. Cell Immunol 2017; 314:63–72.